

Research Article

Integrated Geophysical-Geological 3D Model of the Right-Bank Slope Downstream from the Rogun Dam Construction Site, Tajikistan

Hans-Balder Havenith ¹, Isakbek Torgoev,² and Anatoli Ischuk³

¹Department of Geology, Liege University, Liege, Belgium

²Institute of Geomechanics and Mining, Academy of Sciences, Bishkek, Kyrgyzstan

³Institute of Geology, Earthquake Engineering and Seismology, Academy of Sciences, Dushanbe, Tajikistan

Correspondence should be addressed to Hans-Balder Havenith; hb.havenith@uliege.be

Received 30 March 2018; Revised 18 July 2018; Accepted 2 August 2018; Published 27 August 2018

Academic Editor: Veronica Pazzi

Copyright © 2018 Hans-Balder Havenith et al. This is an open access article distributed under the Creative Commons Attribution License, which permits unrestricted use, distribution, and reproduction in any medium, provided the original work is properly cited.

In summer of 2015 we had completed a geophysical survey complemented by borehole drilling near the right-bank slope of the Rogun Dam construction site, Tajikistan. These data were first processed and then compiled within a 3D geomodel. The present paper describes the geophysical results and the 3D geomodel generated for an ancient mass movement located immediately downstream from the construction site. The geophysical survey included electrical and seismic profiles and ambient vibration measurements as well as earthquake recordings. The electrical and seismic data were processed as tomographic sections, the ambient vibrations as horizontal-to-vertical spectral H/V ratios, and the earthquake data mainly in terms of standard spectral ratios. By estimating the average shear wave velocities of the subsurface, we computed the local soft layer thickness from the resonance frequencies revealed by the H/V ratios. Three seismic stations had been installed for ten days along a profile crossing the intermediate plateau. Standard spectral ratios inferred from ten processed earthquake measurements confirmed the presence of a thick soft material layer on the plateau made of weathered rocks, colluvium, and terrace deposits, which produce a medium-level amplification at about 2 Hz. The 3D geomodel was first built on the basis of new topographic data, satellite imagery, and a geological map with two sections. Then, the various electrical resistivity and seismic refraction tomographies were inserted in the geomodel. The soft layer thickness information and borehole data were represented in terms of logs in the model. The site is crossed by the Ionakhsh Fault that could be modeled on the basis of the geological inputs and of a lateral resistivity gradient found on one electrical profile along the steep lower slope. The integrated interpretation of all results reveals that probably only a relatively small part of the ancient giant mass movement is really exposed to slope instability phenomena.

1. Introduction

The Rogun dam construction site is located in central Tajikistan within the Vakhsh River valley at about 100 km in the Northeast of Tajikistan's capital Dushanbe and 40 km upstream from the Nurek reservoir. The project of the construction of the dam and the associated hydropower plant (HPP) had already started when Tajikistan still belonged to the Soviet Union. It was part of a much wider project of hydropower plant construction that was completed by the Soviet Union in Central Asian countries, including also other dams and HPPs constructed along Vakhsh River in Tajikistan

as well as the large hydropower cascade along Naryn River in Kyrgyzstan (Figure 1). There, the last construction of the (relatively small) Kambarata 2 dam had been completed in 2012; at present, it is the only 'blast-fill' dam within the two hydropower cascades (a full description of the blast event, construction works, and geophysical investigations on the dam is provided by Havenith et al. [1]).

The Rogun dam construction project was relaunched in the beginning of this century (2005) under the present-day's (2018) government. As for many other types of dams, the site for this one had been selected in a very narrow part of the Vakhsh River valley (to reduce the amount of material needed

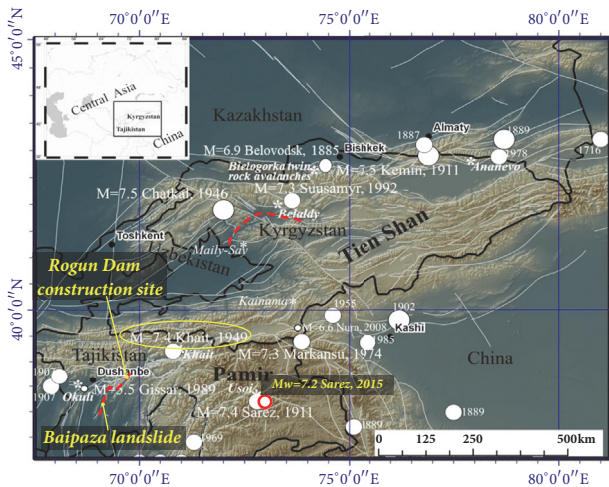


FIGURE 1: Map of Tien Shan and Pamir Mountains in Central Asia with location of major faults and earthquakes (white circles show all recorded $M \geq 6.9$ earthquakes with the year of occurrence; the magnitude is indicated for analysed events) and related major mass movements (stars). Highlighted by red dashed lines are the Naryn HPP cascade in Kyrgyzstan and the one of Vakhsh River in Tajikistan; the locations of the Rogun dam construction site and of the Baipaza landslide, as well as the epicentral areas of the 1949 Khait earthquake and the 2015 Sarez earthquake (red circle) are indicated (modified from Havenith and Bourdeau, 2010).

for construction). The associated Rogun HPP will be part of the cascade of already existing HPPs, including those of Nurek, Baipaza, Sangtuda 1+2, and the “Golovnaya” (head, or final). The Rogun dam, just as Nurek dam, is designed as a rockfill dam with a clay core. At the end of the 70s, Nurek dam had been the tallest dam in the world (with a height of 300 m); right now Nurek is the second tallest one after Jinping-I dam in China. After completion, the Rogun dam would be the future tallest dam on Earth (design height of 335 m).

The present paper is focused on a geophysical survey that had been completed in summer 2015 on a large slope downstream and a smaller one upstream from the Rogun dam construction site. This survey included electrical and seismic profiles as well as ambient noise measurements and earthquake recordings supported by differential GPS positioning (methods are detailed under Section 3). Results from related data processing were then combined in a 3D geomodel of the site. A very similar type of site characterization has been completed with the same methods by Ulysse et al. [2] for a hill site in Port-au-Prince, for which topographic amplification effects had to be assessed.

The objectives of this survey are related to the general hazard situation of the Rogun HPP that is now under construction. The obviously most important regional type of hazard to which the selected site is exposed (just as the other HPP sites downstream) is the one related to earthquakes: the site is located at 100 km in the southwest of the epicentral zone of the catastrophic 1949 Khait earthquake, and at 300-350 km in the West of the 1911 Sarez earthquake (see summary of events in Havenith and Bourdeau [3]). It should be noted that

only a few months after our survey in 2015, the Sarez region was hit by another $M > 7$ earthquake.

At local scale, the site is affected by multiple types of mass movement-related hazards; such hazards are perfectly exemplified by those that had been induced by the two largest aforementioned events, in 1911 and 1949: rock avalanching and river damming. The $M=7.4$ Khait earthquake triggered several large mass movements, including the Khait rock avalanche that had partly covered the town of Khait [4, 5], while the Sarez earthquake triggered a giant rockslide that formed the presently tallest (intact) natural dam on Earth, the Usoy dam [6].

The interest in the slope site downstream from the construction area is also related to the risk of formation of a landslide dam near the exit of the spillway of the Rogun dam. This risk is exemplified by an event that occurred in 2002 near the Baipaza dam and hydropower plant (HPP) that also belong to the Tajik HPP cascade. At that time, a massive failure affected the already existing and identified Baipaza landslide at 4.5 km downstream from the Baipaza HPP (see also Havenith et al. [7]). The first displacement of this landslide had been observed in 1968 when it partially blocked Vakhsh River, even before design and construction of the Baipaza HPP. In 1969, the volume of the Baipaza landslide was assessed to be 20-25 million m^3 . In May, 1992, the Baipaza landslide moved again as a result of heavy rains, and the Vakhsh River was dammed. After the March 3, 2002, deep-focal $M_w=7.4$ Hindu Kush earthquake (with an epicentre located in Afghanistan at a distance 250 km from the Baipaza site, and with an intensity of shaking of 6 degrees on EMS-98 scale), this landslide started to move and partially blocked again the Vakhsh River (Figure 2). As a result, a lake formed upstream from the dam and partly inundated the Baipaza HPP, which could not operate at a normal level for one month. The use of high explosives was required to clear the river bed after this landslide. Note that the view of Baipaza rockslide of 2007 in Figure 2 still shows the presence of the cascade across the dam that had been breached in 2002. Now, the cascade cannot be seen anymore due to river erosion.

As introduced above, the larger downstream zone (Site 1) of the Rogun dam construction site was studied to assess the probability of occurrence of a massive failure event similar to the one observed downstream from Baipaza HPP in 2002; the smaller upstream Site 2 that can be seen on some maps (Figures 6 and 7) was investigated due to the possibility of a potentially tsunamigenic impact of an existing mass movement on the lake. Investigations on both sites are described below (see also Torgoev et al. [8]), with focus on the larger Site 1.

2. The Seismic Hazard and Geological Context of the Dam Site

As seismic hazard maps can provide a more general overview on the seismotectonic activity of a region and its effects on the surface than singular events, and, over a certain period of time, it is important to situate the Rogun site in its regional seismic hazard context. Relatively recent seismic hazard maps for the target region have been produced by Abdrakhmatov

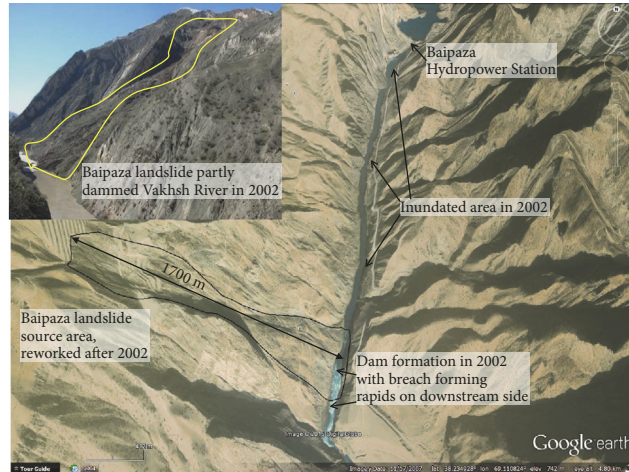


FIGURE 2: Google Earth® view (to N) of the Baipaza rockslide and upstream Baipaza HPP. This image of 2007 still shows the cascade that Vakhsh River formed after crossing the dam that had been formed and actively reopened in 2002.

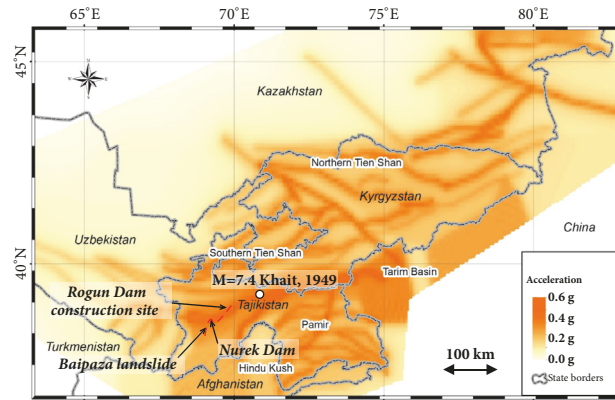


FIGURE 3: Seismic hazard map of the Southeastern part of Central Asia, entirely including the countries of Kyrgyzstan and Tajikistan (modified from Ischuk et al., 2018). Indicated are the locations of the Khait earthquake epicentral region, the Rogun and Nurek sites, and the Baipaza landslide just downstream from the Baipaza HPP.

et al. [11] and Bindi et al. [12], the first one covering only the northernmost part of Tajikistan while the second fully covers Tajikistan. The most recent seismic hazard map has been computed by Ischuk et al. [13]. Actually, Ischuk et al. [13] produced several maps for this part of Central Asia (calculated for a 475-year return period), one considering a 75% contribution by regional (or zonal) and 25% by fault-related seismic ground motion hazards, one considering a 25% regional and 75% fault-related contribution, and the seismic hazard map shown (Figure 3) for a 50% zonal and 50% fault-related contribution. This map shows that the entire Vakhsh hydropower cascade is exposed to a minimum seismic hazard of about 0.3 g. As the Rogun site is located in the northern part of the cascade, it is closer to the active fault zones of the southern Tien Shan, which induce a seismic hazard of even more than 0.4 g (with 10% exceedance probability in 50 years). Comparable high values are displayed on the two other maps (not shown here, the first with stronger regional seismicity and the second with a stronger fault contribution) and were also obtained by the

two other assessments, noting that Bindi et al. [12] expressed their results in terms of Intensities: 7 for the southern part of the Vakhsh HPP cascade and 9 for the northern part.

It should be noted that such large dam structures due to the deep lakes formed upstream are often not only exposed to the effects of natural seismicity, but also to those due to reservoir-triggered seismicity during and just after reservoir filling (generally during the first years after filling—but this could also last longer in the case of Rogun as filling will take a long time and as the lake will be particularly large and deep). For instance, extensive induced seismicity had been observed after the filling of the Nurek reservoir in the 70s [14].

Here, we will not discuss in detail the possible effects of the reservoir-triggered seismicity related to the future filling of the Rogun reservoir. Large-scale effects are generally not expected as a consequence of the reservoir-triggered seismicity, due to the limited magnitudes of related earthquakes ($M < 5$ for the Nurek case); note that exceptional magnitudes of up to 6 had been observed after filling of

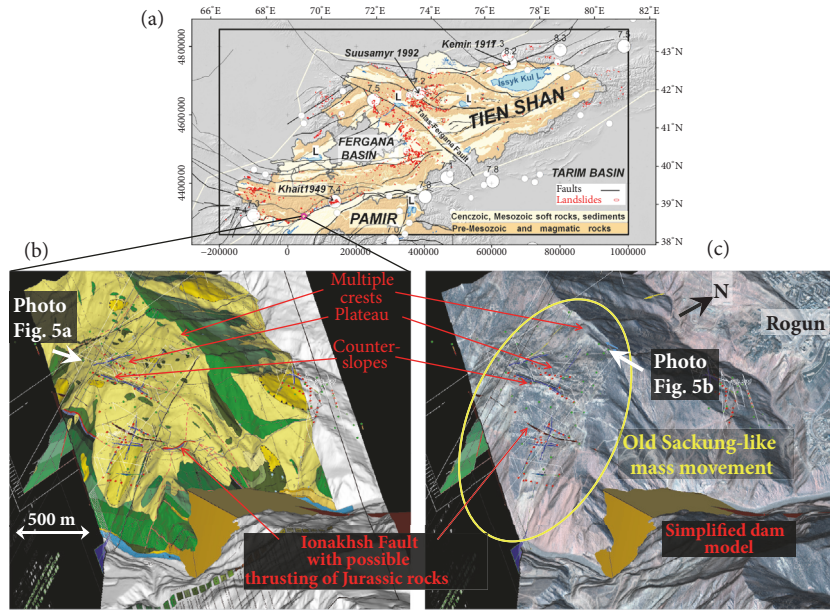


FIGURE 4: Simplified geological map of the Tien Shan (from Havenith et al. [9]). Views of 3D model of site with geological map ((b): green: Cretaceous sandstone bedrock; yellow: quaternary surface deposits, terraces, and colluvium) and a Pleiades image (of September 2015, (c)) projected on the surface, showing also the location of the dam and of the Ionakhsh Fault and elements of the ancient Sackung-like massive slope failure.

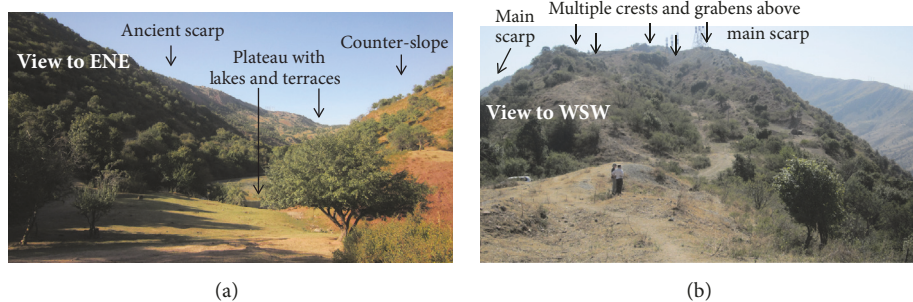


FIGURE 5: Field photographs showing elements of the large ancient Sackung-like mass movement. (see orientation and location of views in Figure 4: (a) view in western part to ENE; (b) view in eastern part to WSW).

the Koyna dam (see paper by Chopra and Chakrabarti [15]). Nevertheless, seismic ground motions can be locally very intense as the hypocentres of those medium-size earthquakes are generally located close to the surface (at depths that can be less than 5 km); if located near the dam structure, shallow $M > 4$ events could cause fractures within the dam (e.g., according to Chopra and Chakrabarti, 1973, the Koyna $M = 6.5$ earthquake had caused damage on the concrete Koyna dam) and neighbouring slopes.

Massive failures along the neighbouring slopes could, however, only occur if a natural $M \geq 7$ earthquake (similar to the aforementioned Khait earthquake) hits the Rogun region. Anyway, the investigations described below were designed to provide inputs for estimates of possible slope failures of multiple origins, induced by purely static (mainly on groundwater pressure depending) factors or by small (or higher frequency) or stronger (lower frequency) seismic ground motions.

The general geological context of the Rogun site is related to its position near the southern border of the Tien Shan. Immediately to the north of the site, the pre-Mesozoic rocks of the Tien Shan are outcropping, while the site itself is located in Mesozoic rocks (see general geological map of the Tien Shan in Figure 4(a)). Most of the right-bank slopes are made of Cretaceous sandstones (green layers in Figure 4(b)) widely covered by colluvium and along the central plateau (see location in Figure 4(c)) also by terrace deposits. Along this plateau also two lakes can be found (one is shown in the photograph in Figure 5(a)). In the central part of the lower slope also upthrust Jurassic clayey rocks can be found. They are markers of the presence of the Ionakhsh Fault that crosses the site from ENE to WSW.

The origin of the intermediate plateau on the right-bank slope downstream from the dam construction site can be explained by an ancient Sackung-like movement of that slope. Another interpretation would be that the

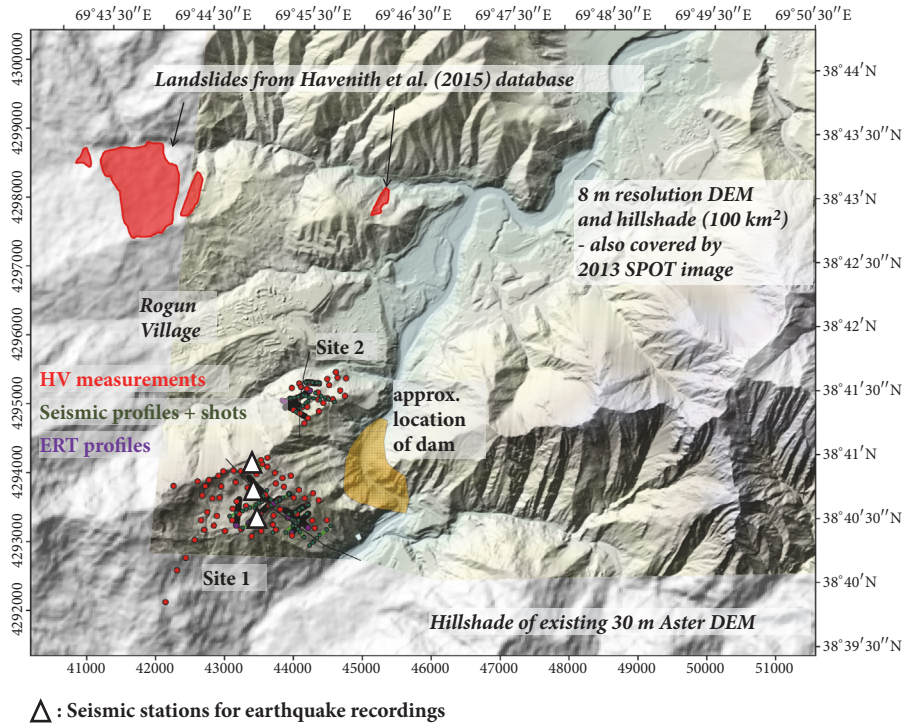


FIGURE 6: Overview of investigated sites with types of measurements indicated. Measurement locations plotted on a hill-shade map, with locations of landslides (reddish) extracted from the geographic-geological database (by Havenith et al. [10]) with overlay of a new 8 m resolution DEM. See detailed site survey views in Figure 8.

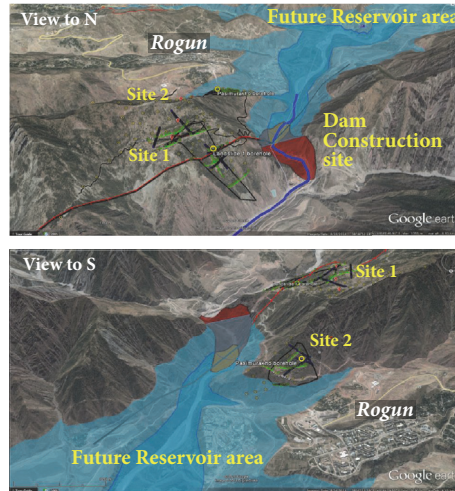


FIGURE 7: Overview of the two investigated sites (Google Earth® views, see detail on types of surveys in Figure 8). Also shown: approximate outlines of the future Rogun dam structure and of the two main reservoir levels (darker and light blue filling of reservoir outlines) after an intermediate and the final construction.

plateau is just the remnant of a river terrace—especially as terrace material is found on this plateau. The interpretation of the whole slope as a major Sackung therefore requires additional elements—the most important one is the presence of multiple crests and graben structures on top of the upper slope (above the plateau, see photograph in Figure 5(b)) that can be considered as the main scarp of the Sackung.

3. The 2015 Rogun Geophysical Field Survey

An overview of the Rogun dam site (in 2015, before the start of dam construction in 2016) and the neighbouring investigated areas is shown in Figures 6 and 7. The first presents an overview map; the second includes Google Earth® imagery views of the investigated sites, with an approximate representation of the future dam structures (that are now being built and would be completed in two stages) and respective lake

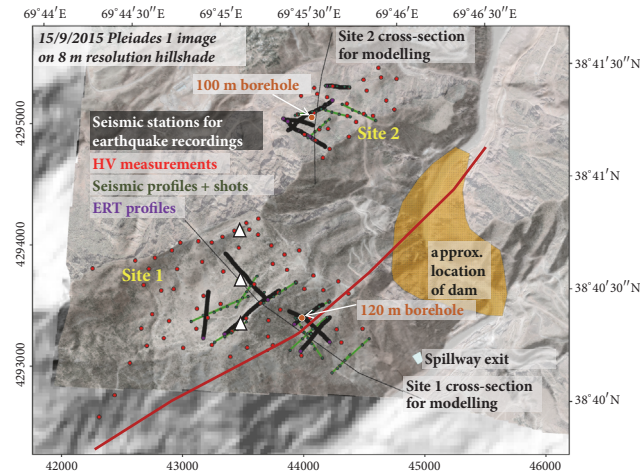


FIGURE 8: Pleiades 2015 satellite image of the surveyed areas outlining types of geophysical measurements and observations: Sites 1 and 2. Black bold lines are electrical resistivity tomography profiles (ERT), green lines are seismic refraction tomography profiles (SRT), red dots are H/V ambient noise measurement points, and triangles are the locations of seismic stations. See also location of the spillway exit (marked by light polygon in lower right corner) and of the boreholes and cross-section that had been used for seismic ground motion simulations and slope stability calculations (not shown in this paper).

levels. A more detailed overview map of the investigated sites with indication of the survey types is shown in Figure 8.

In 2015, our teams had been asked by local officials to study specifically those two sites as both of them present geomorphic features of ancient mass movements: as introduced above, Site 1 presents a terrace-like plateau above the middle part of the slope that could be related to a very old ($\gg 1000y$) massive Sackung; Site 2 has characteristics of an old rockslide with clearly destroyed rock structures. The main “risk” question concerns the reactivation potential of those two ancient massive failures; in this regard, we have to consider that for Site 2 the stability conditions would drastically change with reservoir filling as the toe of the rockslide would be inundated (after complete filling), while for Site 1 the situation will not really change after reservoir filling. The external factor that could contribute to instability on both sites is a major earthquake event near the dam site. Such an earthquake could be either natural as we are located in a seismically active area or induced by the reservoir filling. In both cases, the presence of weak structures such as a fault zone and of groundwater reduces slope stability in general while ground motion amplification effects specifically contribute to the seismic slope failure triggering potential. Therefore, our investigations targeted the detection of both weak zones and wet zones as well as the determination of seismic ground response characteristics. This was achieved through the combination of electrical and seismic methods, combined with seismological measurements.

In total, on both sites up- and downstream from the future dam, we completed a dozen electrical resistivity tomography (ERT) and about the same amount of seismic refraction tomography (SRT) profiles, as well as 92 single station ambient noise (H/V) measurements. In addition to the geophysical measurements, we carried out earthquake recordings during 10 days (only on Site 1); in addition, geotechnical tests were completed on samples collected from two new boreholes (one

120 m deep borehole on Site 1 and one 100 m deep borehole on Site 2).

After processing of all geophysical data, the survey results (including also the borehole data) have been inserted in a 3D geological-geophysical model that was completed with the GOCAD software [16], which will be described in the next section. To support modeling, a new 8 m resolution digital elevation model had been constructed (produced upon order by Apollo Mapping) and new orthorectified high-resolution remote imagery (recent Pleiades and Spot images) had been acquired.

The electrical resistivity survey included 12 ERT profiles (using a GeoTom system with four cables and 100 electrodes) with a total length of 4150 meters and installation of 1035 electrodes (7 profiles on Site 1 and 5 profiles on Site 2, see Figure 8, with some profiles being along the same line to get longer profiles). All electrodes (with a spacing of 4 m between electrodes on all profiles) had been located with a differential GPS (DGPS) with a precision of about 20 cm. For the measurements, we used for all profiles the Wenner array configuration. In the laboratory, data were then processed with the 2D inversion algorithm of Loke and Barker [17] implemented in the RES2DINV software. Four processed ERT profiles on Site 1 are presented in Figure 9.

Examples of ERTs shown in Figure 9 show that the electrical resistivity values are highly variable over Site 1. Along the uppermost profile (ERT near upper scarp, Figure 9(a)) and along the intermediate crest (ERT in Figure 9(b)), relatively high resistivities (>500 ohm.m) were measured all along the investigated profiles. Much lower resistivity values (<100 ohm.m) have been measured along profiles completed on the intermediate plateau (ERT in Figure 9(d)) and along the lower steep slope (ERT in Figure 9(c)). Those lower values are probably indicative both of the presence of soft rocks and/or deposits and of groundwater in the subsoil. Along the plateau it is more likely that these wet soft materials are made

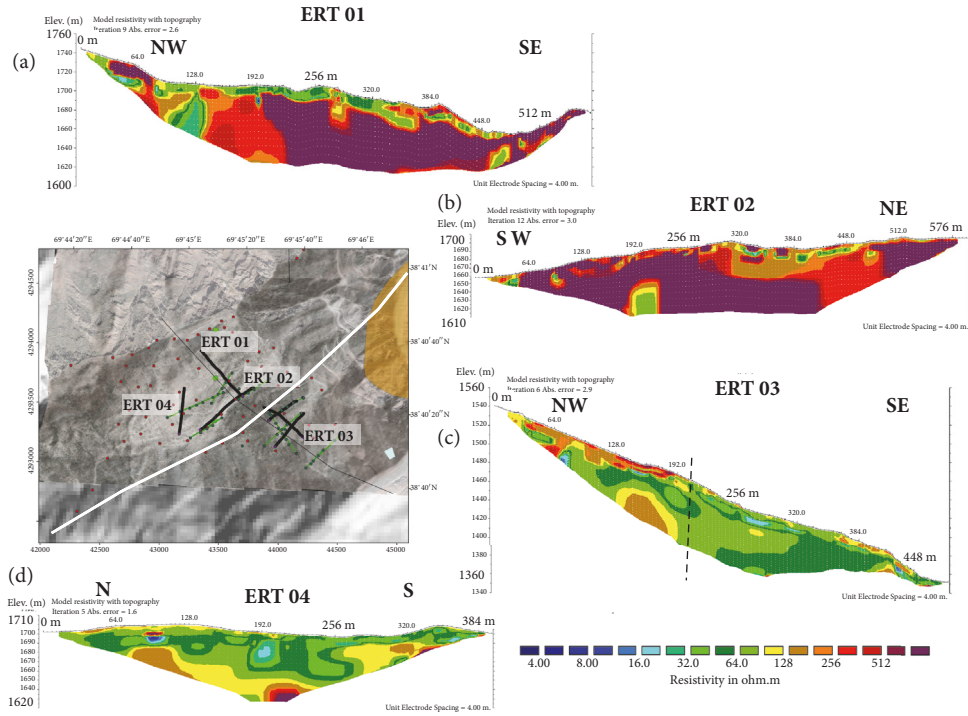


FIGURE 9: Examples of ERT profiles on Site 1 (see resistivity scale in lower right corner, in ohm.m): (a) 576 long ERT in upper part of slope; (b) 576 m long ERT along intermediate slope break; (c) main slope Section 448 m long ERT; (d) near lake-site 384 m long ERT. See in (c) also the dashed line that represents the possible marker of the Ionakhsh Fault crossing the site (shown by white line on the map).

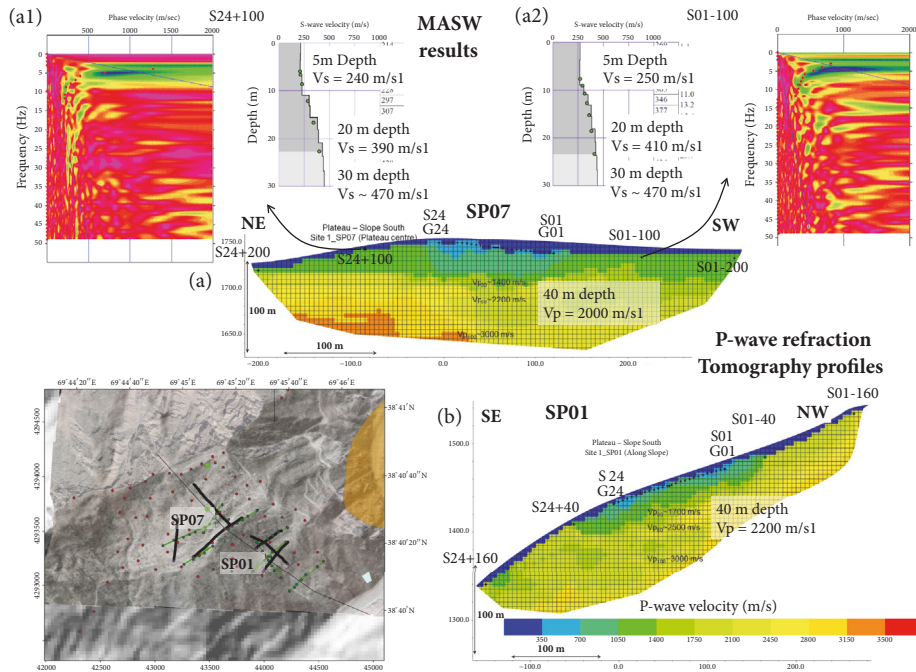


FIGURE 10: Examples of P-wave SRT profiles and MASW results on Site 1: (a) SRT for seismic profile SP07 parallel to the valley orientation, with shots S01 (at 0 m, near first geophone G01) and S24 (at 115 m, near last geophone G24), with 100 m offsets to both sides (S01-100, S24+100) and 200 m offsets (S01-200, S24+200); (a1) and (a2) show MASW results (V_s -logs and surface wave dispersion diagrams) obtained for SP07 for the two 100 m offset shots. (b) SRT for seismic profile SP01 along the main steep slope, with shots S01 (at 0 m, near first geophone G01) and S24 (at 115 m, near last geophone G24), with 40 m offsets to both sides (S01-40, S24+40) and 160 m offsets (S01-160, S24+160). The P-wave velocity scale is shown in lower right corner.

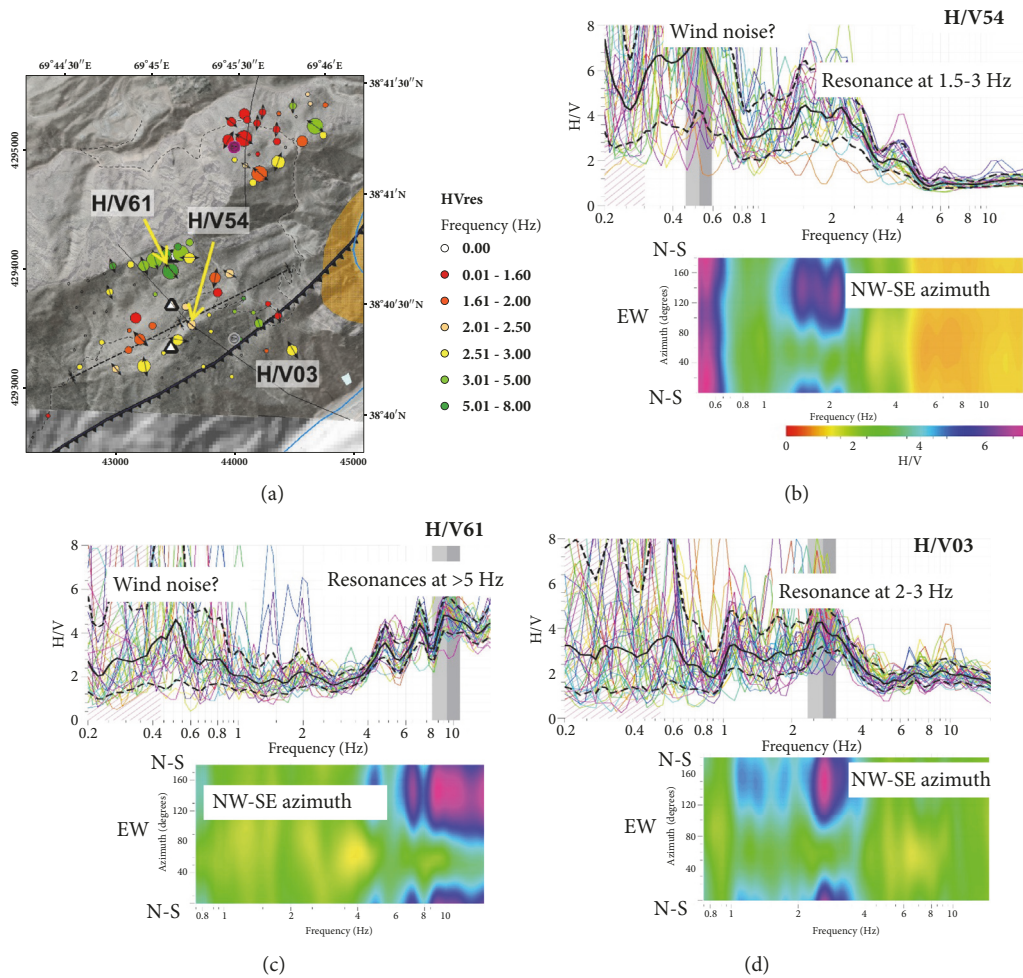


FIGURE 11: (a) Overview map of 92 ambient vibrations measurements (for both studied sites); circles are colored according to the fundamental resonance frequency (see scale in the middle) and with a size proportional to the peak amplitude; see also the double arrows indicating the main vibration orientation (polarization). See also the black Ionakhsh Fault outline crossing the lower slope from NE to SW. (b-d) Three examples of H/V results of processed ambient vibrations, in terms of simple H/V spectral ratios and of H/V azimuth spectra (with polarization information).

of colluvium and/or terrace deposits, while along the slope the material is probably made of wet fractured rocks. We can also see the slight lateral change of resistivities in the middle part of the ERT profile “03” in Figure 9(c), which could point to the presence of a subvertical fault, possibly the Ionakhsh Fault crossing the target region in this area. This lateral change roughly corresponds to the location of the Ionakhsh Fault that is shown on the geological section in Figure 12(c).

The seismic refraction survey included 13 SRT profiles (with Daqlink seismograph and 24 4.5 Hz geophones) with a total length of 4210 meters (8 profiles on Site 1 and 5 profiles on Site 2; see Figure 8). In total, 40 hammer shots and 25 small (250-500 g dynamite) explosions (with min. 40 m offset) were used to trigger seismic waves. Along each profile at least 10 DGPS measurements had been completed to measure the profile position, and all shot points were located by means of DGPS measurements. In the laboratory, the seismic data (recorded over 2.5s, with a time interval of 0.5 ms) were processed with the Sardine software (by

Demanet [18]) in terms of P-wave SRT profiles on Site 1; two examples of SRTs are presented for two long seismic profiles (with several distant explosive shots) in Figure 10. For the seismic profile SP07 (Figure 10(a)) also a multichannel analysis of surface waves (MASW) had been performed (with the SeisImager software, from ABEM company) to determine S-wave velocity (V_s) logs in the middle part of the slope of Site 1 (see V_s -logs and digitized surface wave dispersion diagrams in Figures 10(a1) and 10(a2), respectively, for explosive shots triggered at 100 m from the end and the beginning of the 115 m long profile).

Both SRT profiles in Figure 10 show that in some places relatively low P-wave velocities (V_p) have been measured near the surface, often less than 1000 m/s. These results are also confirmed by low V_s (<500 m/s) measured near the surface, as proved by a few MASW analyses, such as those shown in Figures 10(a1) and 10(a2). Higher V_p -values (>1500 m/s) near the surface were only observed near the upper steep slope below the main crest. At a depth of more than 30 m

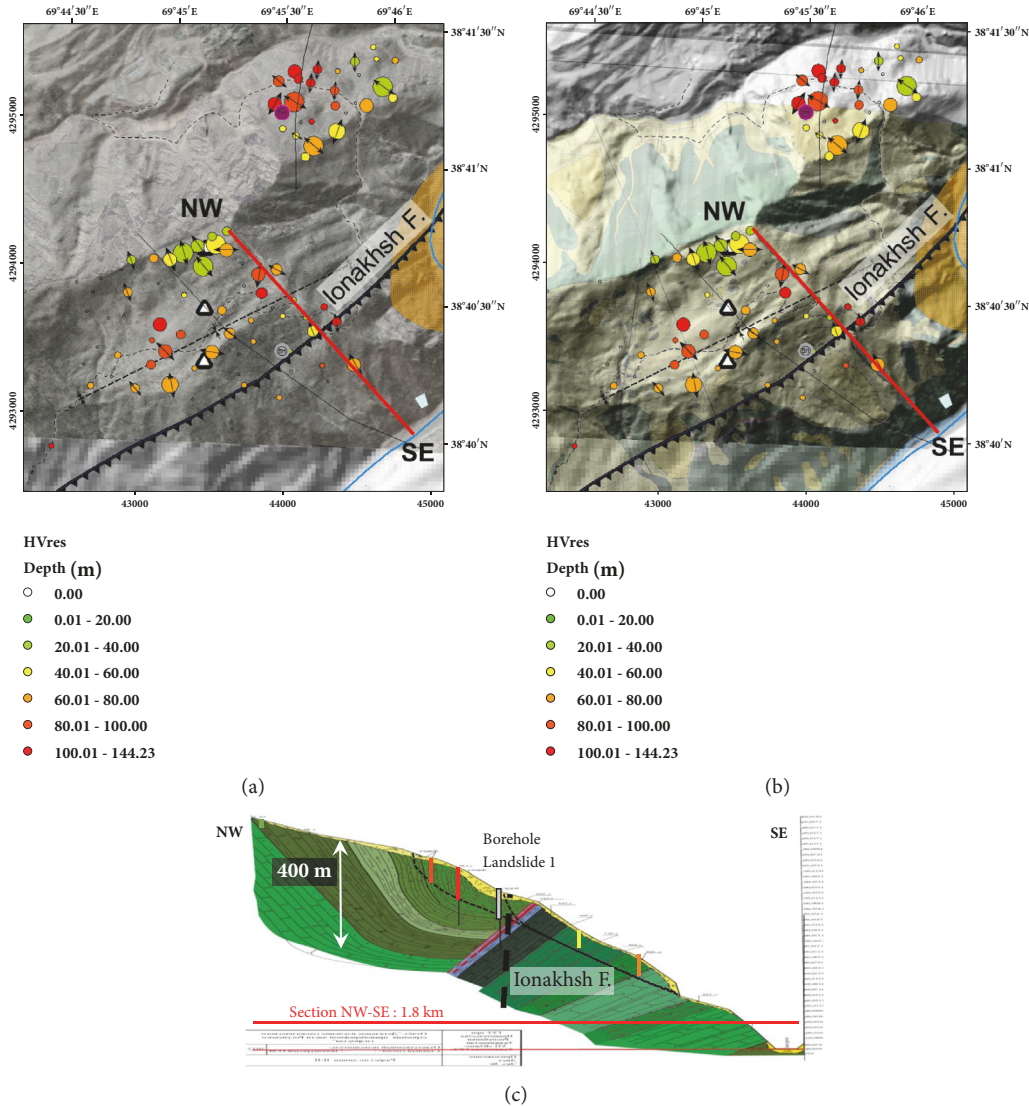


FIGURE 12: (a, b) Overview maps ((a) with Pleiades image; (b) with geological map) of 92 ambient vibrations measurements (for both studied sites); circles are colored according to the depth of the soft rock layer basis inferred from the H/V results and with a size proportional to the peak amplitude; see also double arrows indicating the main vibration orientation (polarization). (c) Geological cross-section (along red line in the maps in (a, b), Southern Tajik Geological Prospecting Expedition, 2012) with location of depth-logs (colored; see for scale the 100 m deep red log) of the soft rock layer basis, location of the Ionakhsh Fault (colored, as from geological map; the dashed black line as inferred from our results), and the borehole (light grey) on Site 1.

only in a few places V_p -values of more than 3000 m/s have been measured. Those results are not typical for a rock slope and point to a general weakening of the rocks over large depths, probably due to intense fracturing. The lowest V_p -values had been measured along the intermediate plateau and along the lower steep slope (see the SRT profiles shown in Figure 10) which are also marked by the lowest electrical resistivities. Thus, for these zones, the presence of deep-seated weak materials has been confirmed by both (electrical and seismic) types of investigations.

By combining all SRT and the two MASW results, we estimated mean V_p - and V_s -values for the first relevant (for slope stability analysis) 60 m, of, respectively, 1500 and 750 m/s (for a Poisson ratio of 0.33) for Site

1 (the values are lower for Site 2, i.e., $V_{p60}=1000$ m, $V_{s60}=500$ m).

92 ambient noise H/V measurements (using a sampling frequency of 200 Hz, completed with a Lennartz L5s seismometer connected to a CitySharkII station) included 62 points on Site 1 and 30 points on Site 2. All H/V points were located with a normal GPS with a precision of about 5 to 7 m. Ambient vibrations data were processed with the Geopsy software (by Wathelet [19]). An overview map of all measurements and three examples of H/V results are shown in Figure 11. The overview map (Figure 11(a)) shows already processed H/V results as circles colored according to the fundamental resonance frequency and with a size proportional to the measured peak amplitude. The three

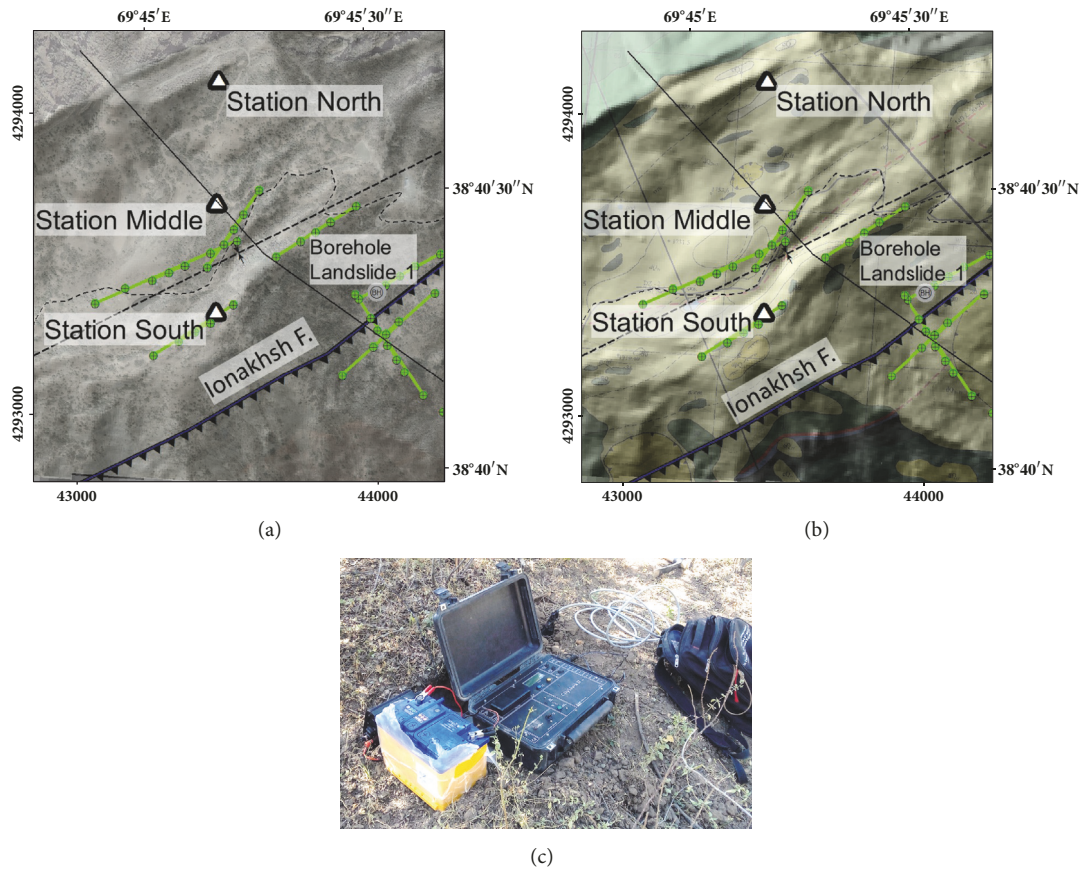


FIGURE 13: (a, b) Overview maps ((a) with Pleiades image; (b) with geological map) of seismological station locations and of seismic profiles (green lines and shot points) on Site 1. (c) CitySharkII station and battery.

examples of H/V results shown in Figures 11(b), 11(c), and 11(d) are presented in terms of both simple H/V spectral ratios and H/V azimuth spectra (with polarization information).

Those examples show that in the upper slope mainly higher resonance frequencies had been measured (>5 Hz, see also green circles in overview map in Figure 11(a), indicating high frequency resonances), marking the presence of a relatively thin (<30 m) cover of potentially weaker materials on top of a medium shallow hard rock, while on the intermediate plateau and also along the steep lower slope some areas are characterized by clear, relatively low frequency, resonance peaks (<4 Hz; see also numerous large red, yellow, and orange circles in those areas in the overview map in Figure 11(a)). Figures 11(b) and 11(c) also show polarization diagrams which clearly indicated a dominant NW-SE oriented shaking of the ambient vibrations, which is likely due to the general NW-SE orientation of the entire slope. In the overview maps in Figure 11(a) and also in Figure 12, this polarization of the horizontal shaking is marked by the azimuth of the double arrows.

From the H/V resonance frequency values, f_0 , we made average soft material thickness, h , estimations, using the equations $h = V_s/4/f_0$. Related results are shown in Figure 12.

For Site 1 we estimate that the thicker soft materials on the intermediate plateau and in some parts of the steep

lower slope mark the general weakness of the rocks in these areas. The map of depths of hard rock indicated by circles is reproduced in Figure 12, together with the same circles plotted on the geological map of the area. Along the red line in Figures 12(a) and 12(b), a geological cross-section (shown in Figure 12(c)) has been established by the Southern Tajik Geological Prospecting Expedition [20]. On this cross-section, we plotted soft layer thickness logs inferred from the H/V resonance frequencies. By interpolating the bottoms of these logs, the body of soft material most exposed to instability phenomena (indicated by a fine dashed line) can be outlined. By comparing H/V results with the geological data, we can also see that the deepest logs are located in the center of a syncline structure within the bedrock. In the middle of this syncline a thick deposit of colluvium/terrace material is marked by the yellow layer in Figure 12(c). Additionally, the 2012 geological survey identified a fault zone in the SE of the Syncline center; this fault zone has also been detected in at least one of our ERT profiles (the one shown in Figure 9(c)); according to our estimates, this fault zone should be subvertical while the geological survey assumed a NW-oriented dip. However, more detailed investigations would be necessary to confirm the precise location of the fault, its dip, and the presence of a certain amount (still uncertain) of Jurassic clayey rocks along the fault.

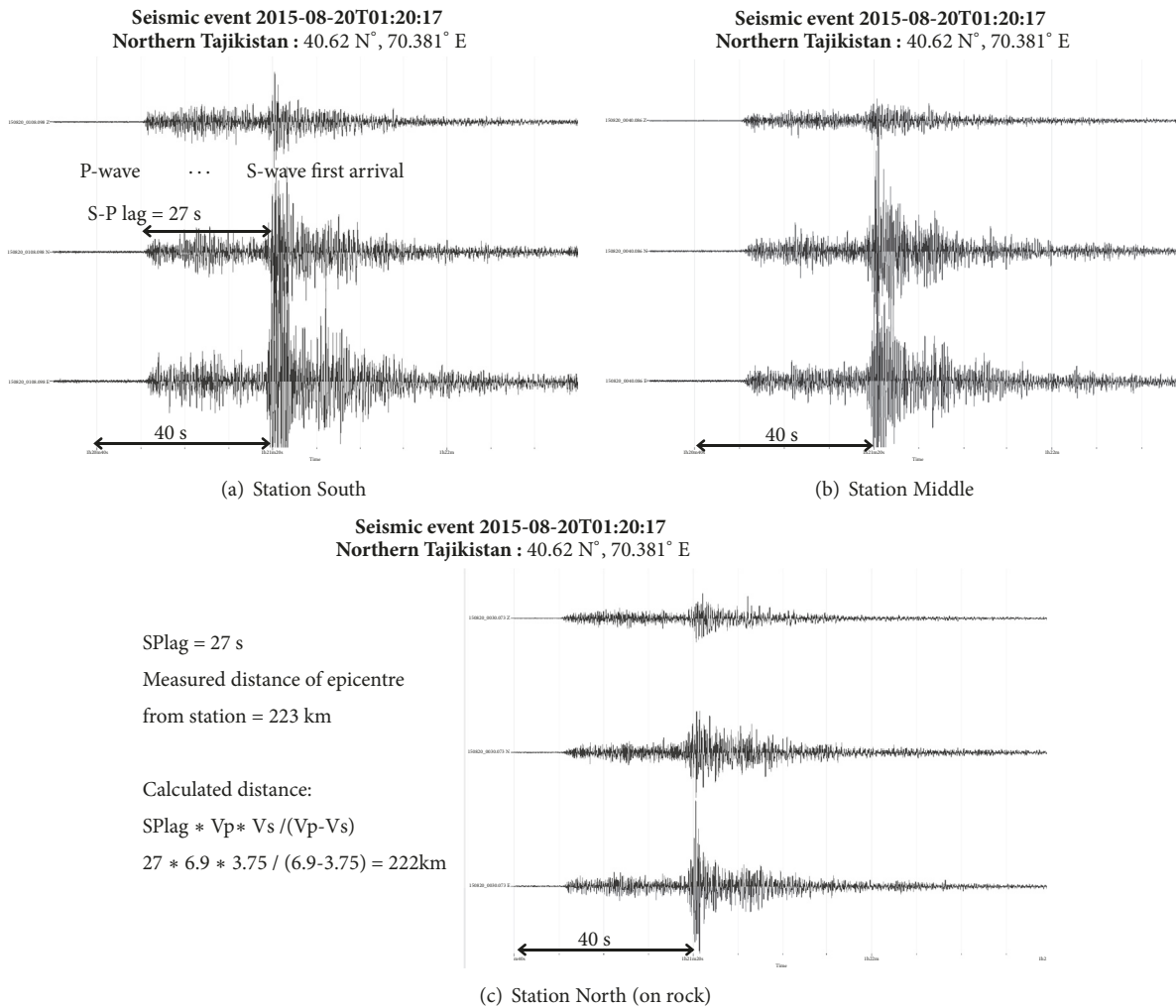


FIGURE 14: Example of seismic event (August 20, 2015, 01:20:17 UTC) in Northern Tajikistan recorded on all three stations: (a) near slope break in the south; (b) on flat area behind the lake; (c) near crest, on hard rock in the north. Amplitudes are scaled.

Seismological recordings have been completed during 10 days with three mobile seismic stations (3 CitySharkII stations, two connected to a Lennartz LIHz seismometer and one connected to an L5s seismometer; see location in Figure 13) in the area of the intermediate plateau, near the central part of the Syncline structure. During this period of seismic observations, a total of 20 earthquakes had been recorded within a distance of 450 km from the site, including 15 seismic events, which had been measured simultaneously by all three seismic stations; according to the Tajik catalogue, 4 events had a magnitude of 4 or larger. The data recorded on/near the plateau (Stations Middle and South in the maps of Figure 13) had been processed in terms of standard spectral ratios (SSR) computed with the Geopsy software with respect to the measurements on a hard rock site above the slump area (Station North in the maps in Figure 13, with the highest location where a CitysharkII station with an LIHz had been installed).

From the common 15 identified earthquake recordings we finally selected 10 events that produced the strongest

amplitudes on our sites. Figure 14 presents an example of an event of 20/08/2015 at 0120 am UTC that was recorded by all three stations. This figure also explains the calculation of epicentral distance on the basis of S-P time lag (time difference between P-wave and S-wave arrival) and estimated average values of V_p and V_s for the Earth crust ($V_p=6.9$ km/s and $V_s=3.75$ km/s for all events with epicentral distance smaller than 300 km and $V_p=7$ km/s and $V_s=4$ km/s for more distant events), estimations being based on calibration with the 4 known event locations (included in the Tajik catalogue). The comparison between those recordings shows that the Southern and Middle Stations are affected by larger shaking amplitudes (here unit-less, but scaled to the same maximum) than the Northern Station that is actually located on (shallow) bedrock.

The spectral analysis applied to the event of 20 August 2015 at 0120 am is documented in Figure 15. This figure shows that the H/V ratios and spectral amplitudes are clearly the smallest at Station North located near outcropping bedrock, which may thus be used as reference station

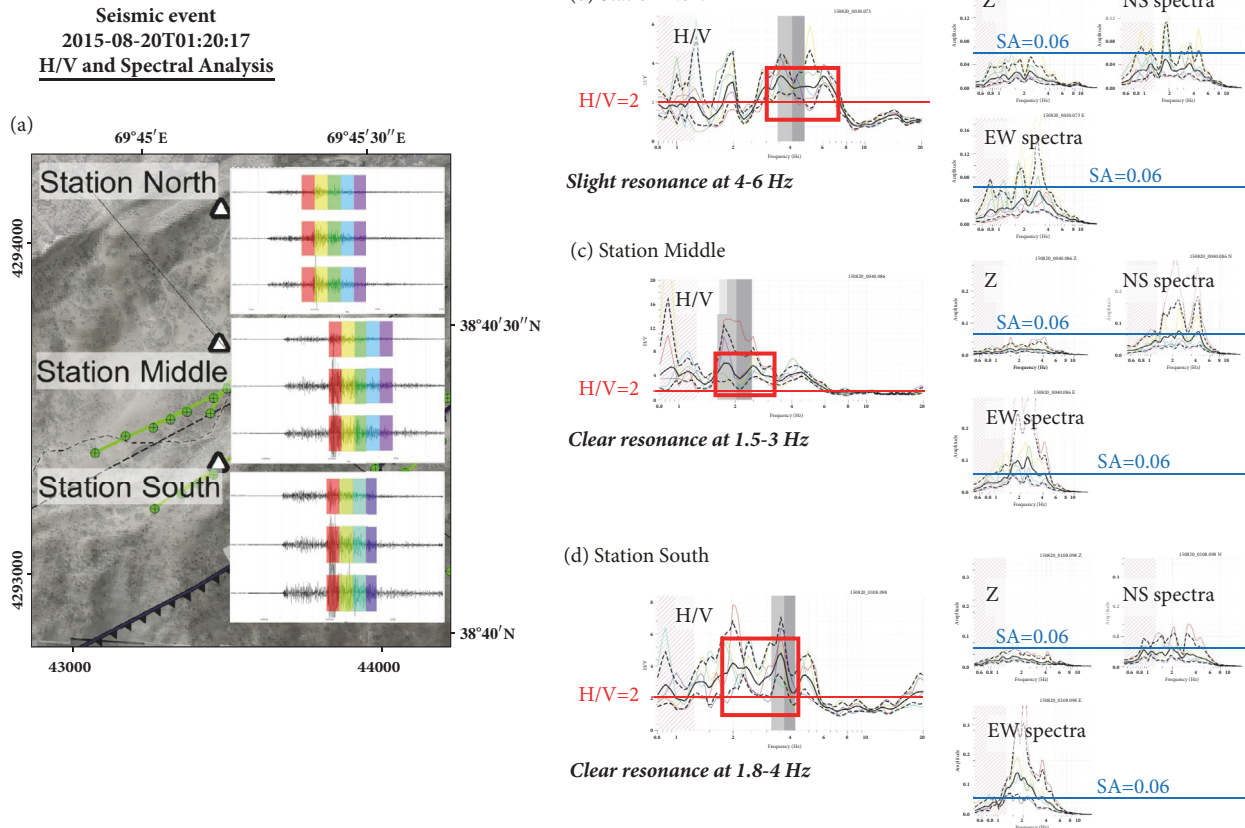


FIGURE 15: August 20, 2015, event analysed with Geopsy software: (a) map with plots of seismograms and 5 selected S-wave windows for spectral analysis; H/V spectral ratios (left) and amplitude spectra (right) calculated for 5 S-wave windows, for Station North (b), Station Middle (c), and Station South (d). See indicated H/V level = 2 and Spectral Amplitude, SA = 0.06.

for site amplification analyses applied to the two other stations.

For each of the 10 analysed events, average EW-NS spectral ratios were computed for Station Middle and Station South with respect to the reference Station North. The procedure is schematically described in Figure 16.

Then, the average of all ten ratios has been computed to determine the site amplification at Station Middle and Station South, as shown in Figure 17. The final average ratios for both Stations Middle and South reveal that the main site amplification (of about 2-3) appears at around 1.5-2.5 Hz (as already shown by the H/V ratios in Figure 11). The strongest amplification is observed for Station Middle (~3) that can only be explained by the presence of deep weak rocks, possibly covered by loose deposits.

Two boreholes had been drilled in autumn 2015, a 120 m deep borehole on Site 1 and a 100 m deep borehole on Site 2. Every 10 m rock samples were taken from the borehole. In total 14 rock samples were used for geotechnical tests completed in two geotechnical laboratories (one belonging to the Rogun HPP construction company and one belonging to the Institute of Geomechanics and Mining of the National Academy of Sciences of the Kyrgyz Republic).

On the basis of the developed 3D geomodels and geotechnical data, slope stability calculations and seismic ground

motion simulations had been completed with the UDEC (Itasca) software. However, those simulations are not the target of the present publication; therefore, below, we will only present some views of the 3D geomodel that has been used as a basis to establish the 2D numerical models.

4. Integrated Geophysical 3D Models and Rock Fall Simulations

All data processed have been inserted in a 3D geological-geophysical model completed with the GOCAD software. The core of the 3D Geomodel is the digital elevation surface model extracted from the 2D GIS software in point format and reinterpolated in GOCAD (as 3D surface). Raster mapping data such as geological maps and satellite images were then projected on this 3D surface (see upper parts of Figures 18 and 19). All geophysical profiles and geological sections (by Southern Tajik Geological Prospecting Expedition, 2012) were imported as vertical Raster profiles disposed in the right position; in addition, all H/V soft layer thickness logs have been inserted as vertical borehole logs (see lower parts of the Figures 18 and 19). In addition, we represented a section of the Ionakhsh Fault in the model (brown surface in the lower parts in Figures 18 and 19); the 3D views show that this fault would cross the middle-upper part of the Southern

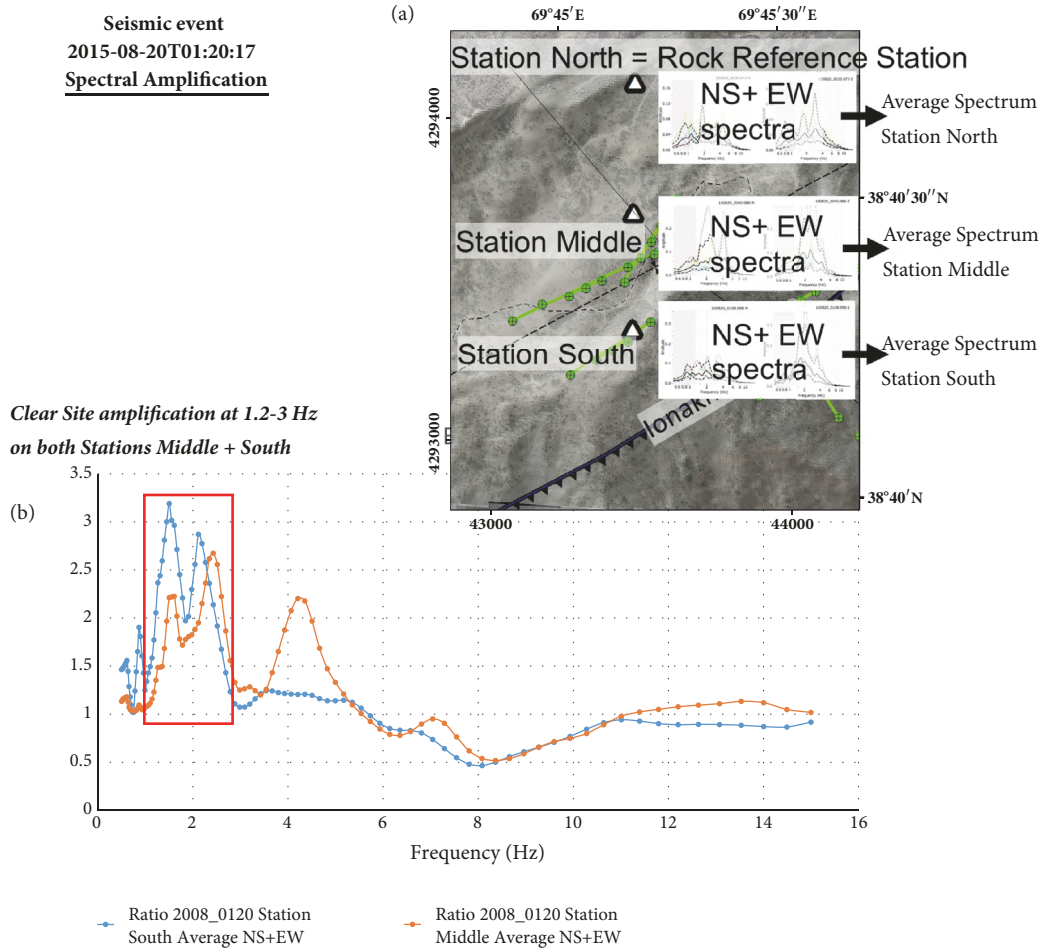


FIGURE 16: Spectral ratios for averaged NS and EW spectra (from spectra shown in Figures 15(b)– 15(d)) computed for event of August 20, 2015 (UTC 01:02:17) for Stations South and Middle with respect to Station North (used as reference station). Location of stations and type of processing indicated in (a); resulting spectral ratios for Station South (blue curve) and Middle (orange curve), with Station North as reference shown in (b).

Slope of Site 1 (denoted as “Landslide 1” in Figures 18 and 19).

A closer view showing the spatial relationship between the Ionakhsh Fault, the site geometry, geophysical profiles, and the existing geological sections is shown in Figure 18. Here, we can see that one ERT profile along the slope crosses the fault (see yellow bar in yellow outline). The large along-slope seismic tomography also crosses the fault (see lower parts of Figures 19(a) and 19(b)), but outside the location of geophones where the V_p variations are weakly controlled. Therefore, no particular V_p changes are shown by this long seismic tomography as all geophones are located on the East side of the fault. However, the ERT profile (shown in Figure 9(c)) displays a change of resistivity from low resistivity in the East (<60 ohm.m) to medium resistivity in the West (>130 ohm.m). This contact seems to be subvertical. Also, our observations in the field combined with analyses of satellite images (Pleiades) confirm a roughly vertical contact of outcropping reddish sandstones in the East (lower Cretaceous) to outcropping grey sandstones in the West (Upper Cretaceous, also found in the borehole). So, we do

not follow the interpretation of the Southern Tajik Geological Prospecting Expedition [20] indicating a fault dip (of less than 60°) to the Northwest (see red line on their profile in Figure 12). The consequence is that, with a vertical dip, the fault also crosses a major part of the upper dam slope (while it would barely “touch” the dam if a dip to the NW is assumed). However, as indicated above, a series of uncertainties affect those interpretations; to confirm the strike and dip of the fault more detailed investigations would have to be completed on the site (also to the East and West of the main slope).

5. Discussion and Conclusions

The main result of the geophysical survey (combined with geological data that were briefly introduced above) is the identification of a large weak zone (roughly 800 by 450 m, along the steep lower slope, starting above the intermediate slope break) on the main investigated Site 1 that is outlined in yellow in the 3D geomodel views in the Figures 18 and 19.

This conclusion is based on previous studies summarized in the report of the Southern Tajik Geological Prospecting

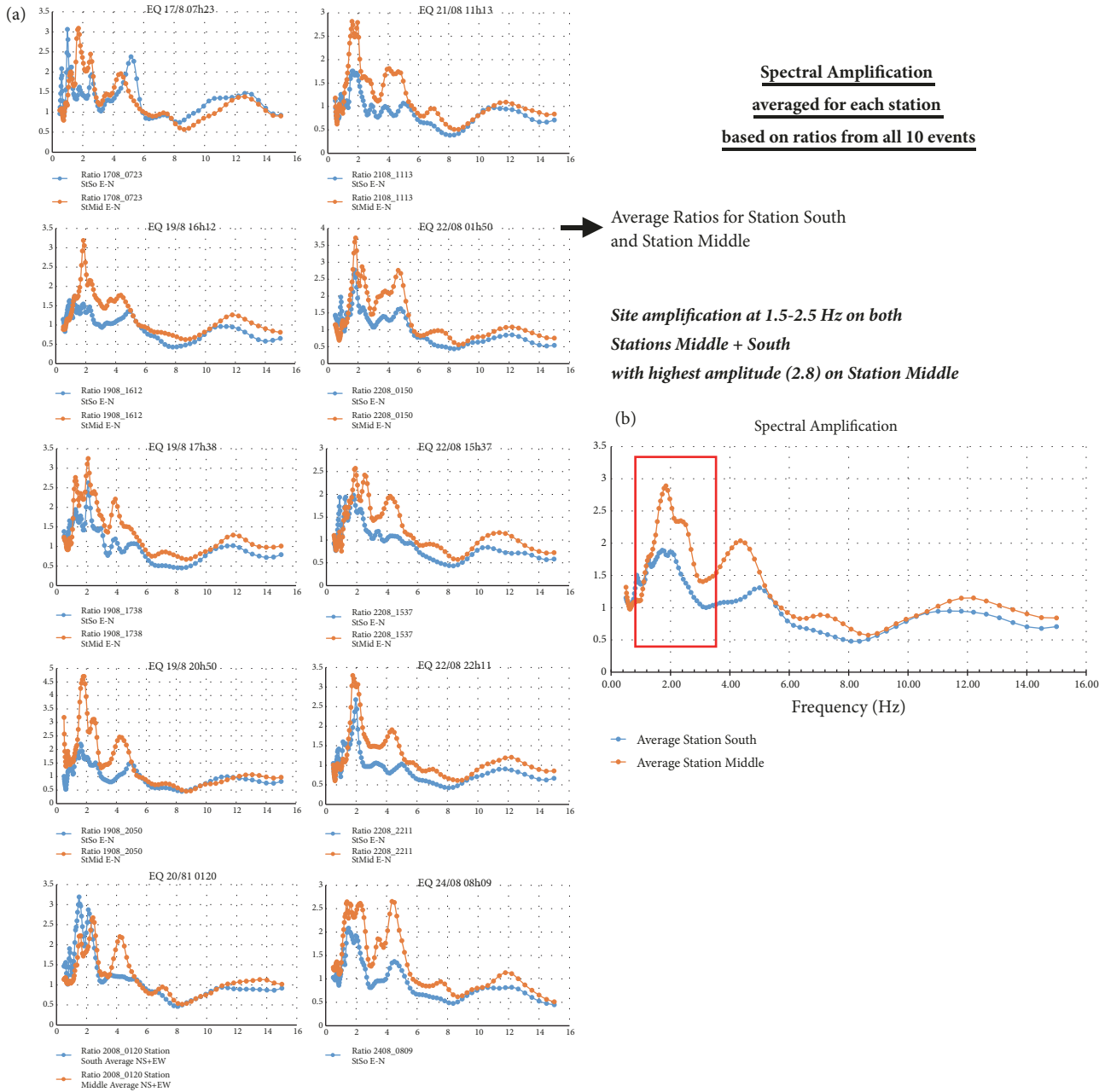
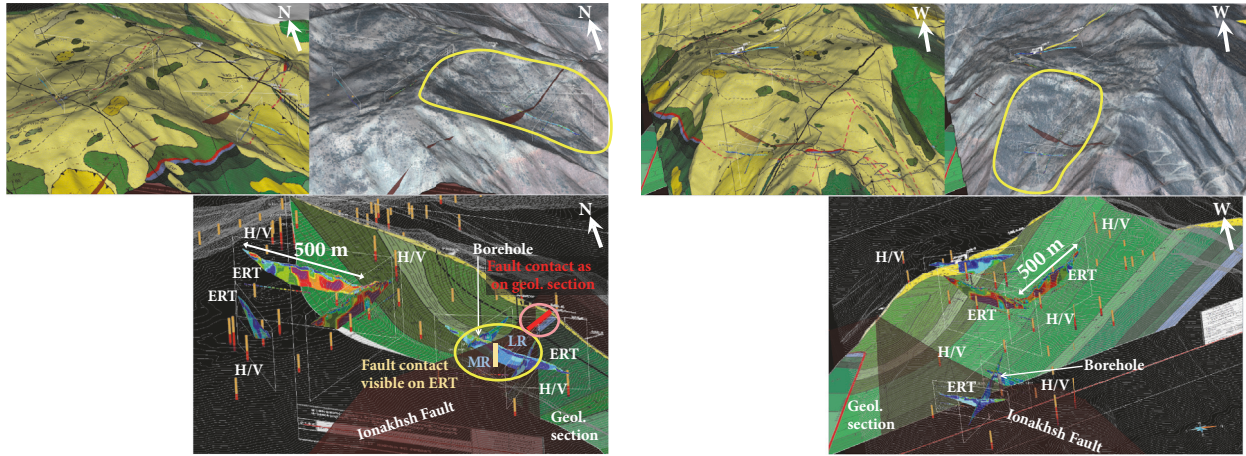


FIGURE 17: (a) Spectral ratios for averaged NS and EW spectra computed for 10 events recorded on all 3 stations, for Stations South and Middle with respect to Station North (used as reference station). (b) Final average spectral ratios for combined NS and EW spectra (from all 10 events), for Stations South (blue curve) and Middle (orange curve) with respect to Station North (used as reference station).

Expedition [20], combined with our geophysical results. The past studies highlighted the morphological and structural features of Site 1, on the right-bank slope of the Vakhsh River above the spillway exit of the Rogun HPP, which characterize a very large potentially unstable zone. Those studies concluded that the total area of the right-bank slope exposed to landslide processes would be about $1.4 \cdot 10^6 \text{ m}^2$ ($1700 \cdot 800 \text{ m}$: this includes the entire plateau and upper steep slope); the unstable mass would have a thickness of up to 500 m; consequently, the total volume of this mass could be up to $700 \cdot 10^6 \text{ m}^3$. Actually, these estimates are close to

ours when we consider the whole ancient mass movement covering almost the entire investigated slope.

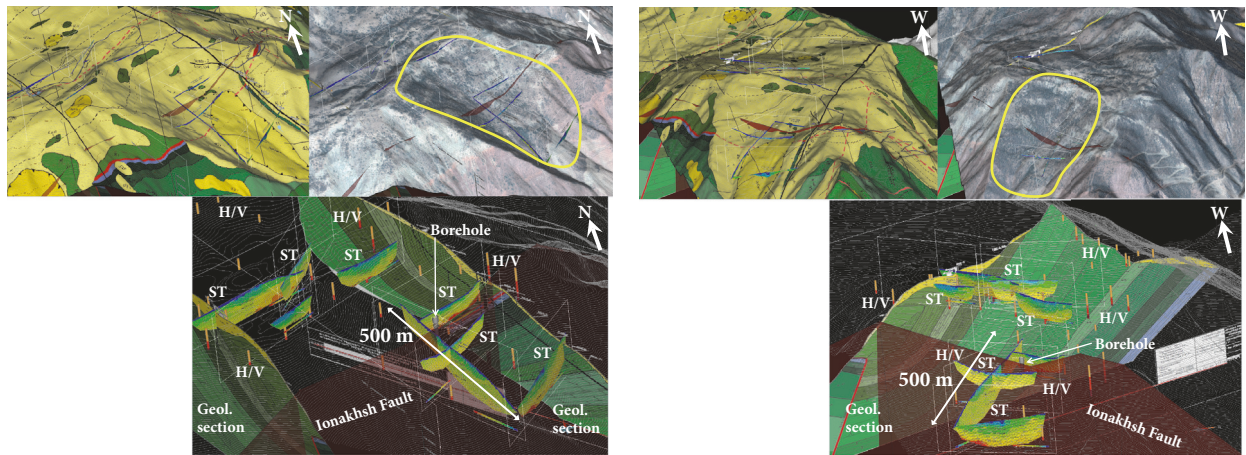
Within this zone, our geophysical results confirmed the presence of a soft layer (weak material) near the surface. However, the extent of the area that is really marked by unfavorable geophysical properties (low resistivity values of less than 100 ohm.m observed in several parts of the intermediate plateau and along the lower steep slope, V_p and V_s of, respectively, less than 1000 and 500 m/s, up to a depth of 20 m as well as low resonance frequencies of less than 4 Hz in the same zones) is far less than what has been estimated



(a) Rogun Geomodel—sections, Landslide 1: ERT from SSW

(b) Rogun Geomodel—sections, Landslide 1: ERT from E

FIGURE 18: Views of 3D geomodel for Site 1 with location of ERT profiles, geological sections, Ionakhsh Fault, H/V logs, and borehole log ((a) view from SSW; (b) view from E). The yellow outline (~800 m long, ~450 m wide) marks the zone that we estimate to be most exposed to slope instability phenomena.



(a) Rogun Geomodel—sections, Landslide 1: SRT from SSW

(b) Rogun Geomodel—sections, Landslide 1: SRT from E

FIGURE 19: Views of 3D geomodel for Site 1 with location of SRT profiles, geological sections, Ionakhsh Fault, H/V logs, and borehole log ((a) view from SSW; (b) view from E). The yellow outline (~800 m long, ~450 m wide) marks the zone that we estimate to be most exposed to slope instability phenomena.

by previous studies and of the amount of $350 \cdot 10^3 \text{ m}^2$ (800 by 450 m yellow outline in the Figures 18 and 19). Figure 14(c) shows that this unstable mass can locally have a thickness of up to 100 m, but on average it is 20-40 m thick. According to those data, the volume of the unstable mass could be up to $10\text{-}15 \cdot 10^6 \text{ m}^3$.

Certainly, also our estimates are affected by numerous uncertainties. First of all, all geophysical measurements highlighted the great variability of electrical, seismic, and resonance properties over Site 1. We observed an absence of resonance peaks in the western part (roughly in the west of the lake of the plateau) which hints at the presence of outcropping hard rock, while along the slope break of the plateau and all over the eastern part of Site 1, resonance frequencies of 1 to 4 Hz indicate the presence of more deeply

fractured-weathered rocks with possible presence of soft deposits (colluvium as well as the terrace material on the plateau). This information combined with morphological aspects such as the deep graben-like depression along the southern border of the plateau might indicate the presence of a deep-seated instability responsible for a more intense fracturing of this part of the slope compared to the western zone. Most probably the Ionakhsh Fault crossing the site and identified on one of the ERT profiles (with subvertical dip) would also contribute to the general instability of the steepest part of the southern slope and of the border of the plateau above the same.

Here, we have not presented the outcomes of numerical studies that had been completed to estimate the likelihood that a major mass movement could be triggered from Site 1

(see a short summary in Havenith et al. [21]). Also, the main question at the origin of our study has not been answered in this paper that is focused on the geophysical results obtained for Site I: could a major mass movement that may be triggered by an earthquake also form a dam on Vakhsh River and could the dammed lake block the exit of the spillway tunnel? We intend to publish those results in a follow-up paper.

Data Availability

The geophysical data used to support the findings of this study are available from the corresponding author upon request.

Conflicts of Interest

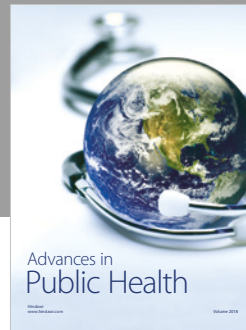
The authors declare that they have no conflicts of interest.

Acknowledgments

These works had been completed in 2015 and 2016 in the frame of the ‘Program of comprehensive geophysical exploration, analytical calculations and modeling potential stability of the landslide-prone slopes in the area of the main facilities of the Rogun HPP’, under the Contract No. 2015-5/2-OP. We thank the Joint Stock Company ‘Rogunskaya GES’ for having allowed us to complete the geophysical surveys on the sites 1 and 2 and for having provided access to past reports.

References

- [1] H. Havenith, I. Torgoev, A. Torgoev, A. Strom, Y. Xu, and T. Fernandez-Steeger, “The Kambarata 2 blast-fill dam, Kyrgyz Republic: blast event, geophysical monitoring and dam structure modelling,” *Geoenvironmental Disasters*, vol. 2, no. 1, 2015.
- [2] S. Ulysse, D. Boisson, C. Prépetit, and H. Havenith, “Site Effect Assessment of the Gros-Morne Hill Area in Port-au-Prince, Haiti, Part A: Geophysical-Seismological Survey Results,” *Geosciences*, vol. 8, no. 4, p. 142, 2018.
- [3] H.-B. Havenith and C. Bourdeau, “Earthquake-induced landslide hazards in mountain regions: A review of case histories from Central Asia,” *Geologica Belgica*, vol. 13, no. 3, pp. 137–152, 2010.
- [4] N. N. Leonov, “The Khait, 1949 earthquake and geological conditions of its origin,” in *Proceedings of the Academy of Sciences of the USSR, Geophysics*, vol. 3, pp. 409–424, 1960 (Russian).
- [5] S. G. Evans, N. J. Roberts, A. Ischuk, K. B. Delaney, G. S. Morozova, and O. Tutubalina, “Landslides triggered by the 1949 Khait earthquake, Tajikistan, and associated loss of life,” *Engineering Geology*, vol. 109, no. 3–4, pp. 195–212, 2009.
- [6] R. L. Schuster and D. Alford, “Usoi landslide dam and Lake Sarez, Pamir Mountains, Tajikistan,” *Environmental and Engineering Geoscience*, vol. 10, no. 2, pp. 151–168, 2004.
- [7] H. B. Havenith, K. Abdrakhmatov, I. Torgoev et al., “Earthquakes, Landslides, Dams and Reservoirs in the Tien,” in *Landslide Science and Practice*, C. Margottini, P. Canuti, and K. Sassa, Eds., pp. 27–31, 2013.
- [8] I. Torgoev, H.-B. Havenith, A. Torgoev, P. Cerfontaine, and A. Ischuk, “Geophysical investigation of the landslide-prone slope downstream from the Rogun Dam construction site (Tajikistan),” in *Culture of Living with Landslides*, M. Mikos, N. Casagli, Y. Yueping, and K. Sassa, Eds., vol. 4, pp. 75–84, 2017.
- [9] H. B. Havenith, A. Torgoev, R. Schlögel, A. Braun, I. Torgoev, and A. Ischuk, “Tien Shan Geohazards Database: Landslide susceptibility analysis,” *Geomorphology*, vol. 249, pp. 32–43, 2015.
- [10] H. B. Havenith, A. Strom, I. Torgoev et al., “Tien Shan Geohazards Database: Earthquakes and landslides,” *Geomorphology*, vol. 249, pp. 16–31, 2015.
- [11] K. Abdrakhmatov, H.-B. Havenith, D. Delvaux, D. Jongmans, and P. Trefois, “Probabilistic PGA and Arias Intensity maps of Kyrgyzstan (Central Asia),” *Journal of Seismology*, vol. 7, no. 2, pp. 203–220, 2003.
- [12] D. Bindi, K. Abdrakhmatov, S. Parolai et al., “Seismic hazard assessment in Central Asia: Outcomes from a site approach,” *Soil Dynamics and Earthquake Engineering*, vol. 37, pp. 84–91, 2012.
- [13] A. Ischuk, L. W. Bjerrum, M. Kamchybekov, K. Abdrakhmatov, and C. Lindholm, “Probabilistic seismic hazard assessment for the area of Kyrgyzstan, Tajikistan, and eastern Uzbekistan, central Asia,” *Bulletin of the Seismological Society of America*, vol. 108, no. 1, pp. 130–144, 2018.
- [14] D. W. Simpson and S. K. Negmatullaev, “Induced seismicity at Nurek Reservoir, Tadjikistan, USSR,” *Bulletin of the Seismological Society of America*, vol. 71, no. 5, pp. 1561–1586, 1981.
- [15] A. K. Chopra and P. Chakrabarti, “The Koyna earthquake and the damage to Koyna dam,” *Bulletin of the Seismological Society of America*, vol. 63, no. 2, pp. 381–397, 1973.
- [16] Paradigm, “Paradigm R - E&P Subsurface Software Solutions,” <http://www.pdgm.com/>.
- [17] M. H. Loke and R. D. Barker, “Practical techniques for 3D resistivity surveys and data inversion,” *Geophysical Prospecting*, vol. 44, no. 3, pp. 499–523, 1996.
- [18] D. Demanet, *Tomographies 2D et 3D à partir de mesures géophysiques en surface et en forage [Ph.D. thesis]*, Liege University, Belgium, 2000.
- [19] M. Wathelet, “GEOPSY Geophysical Signal Database for Noise Array Processing. Software, LGIT, Grenoble, Fr,” <http://www.geopsy.org>.
- [20] Southern-Tajik Geological Prospecting Expedition, *Detailed Study of Geological Structure of The Right Bank of Rogun Hydro-system*, vol. 81, 2012.
- [21] M. Mikoš, N. Casagli, Y. Yin, and K. Sassa, *Advancing Culture of Living with Landslides*, Springer International Publishing, Cham, 2017.



Hindawi

Submit your manuscripts at
www.hindawi.com

